

Composite action of hollow concrete-filled circular steel tubular stub columns

Qiang Fu¹, Fa-xing Ding¹, Tao Zhang^{*1}, Liping Wang¹ and Chang-jing Fang^{1,2,3}

¹ School of Civil Engineering, Central South University, Changsha, Hunan Province, 410075, P.R. China

² National Engineering Laboratory for High Speed Railway Construction, Changsha, 410075, P.R. China

³ Engineering Technology Research Center for Prefabricated Construction Industrialization of Hunan Province, 410075, P.R. China

(Received September 22, 2017, Revised January 3, 2018, Accepted January 11, 2018)

Abstract. To better understand the influence of hollow ratio on the hollow concrete-filled circular steel tubular (H-CFT) stub columns under axial compression and to propose the design formula of ultimate bearing capacity for H-CFT stub columns, 3D finite element analysis and laboratory experiments were completed to obtain the load-deformation curves and the failure modes of H-CFT stub columns. The changes of the confinement effect between core concrete and steel tube with different hollow ratios were discussed based on the finite element results. The result shows that the axial stress of concrete and hoop stress of steel tube in H-CFT stub columns are decreased with the increase of hollow ratio. After the yield of steel, the reduction rate of longitudinal stress and the increase rate of circumferential stress for the steel tube slowed down. The confinement effect from steel tube on concrete also weakened slowly with the increase of hollow ratio. Based on the limit equilibrium method, a simplified formula of ultimate bearing capacity for the axially loaded H-CFT stub columns was proposed. The predicted results showed satisfactory agreement with the experimental and numerical results.

Keywords: hollow ratio; ultimate bearing capacity; finite element method; composite action

1. Introduction

In recent years, concrete-filled steel tube (CFT) is widely used in bridges and buildings. Due to the benefit of composite action of the two materials, the CFT columns show excellent structural performance such as high strength, high ductility and large energy absorption capacity, which were demonstrated in literatures (Chang *et al.* 2013, 2014, Ellobody 2013a, b, Lai and Ho 2013, Hua *et al.* 2014, Feng *et al.* 2015, Qu *et al.* 2015, Albaredavalls and Carreras 2015, Aslani *et al.* 2015, 2016, Patel *et al.* 2016). The hollow concrete-filled steel tubular (H-CFT) section is made by utilizing the centrifugal action of centrifuge to fill with a certain thickness of concrete on the inner wall of a circular steel tube (as shown in Fig. 1). Compared to the conventional CFT, H-CFT has the merits of concrete-saving and convenient for installation of building services. The H-CFT sections has been widely applied in electricity transmission towers regarding that the central hollow part of the H-CFT can be used to place various pipelines and other facilities.

The hollow concrete-filled steel tubular section has gained attention of researchers since decades ago. Kuranovas and Kvedaras (2007) reported the experimental studies for the ultimate bearing capacity of H-CFT stub columns under axial compression, in which the differences between the solid and hollow concrete-filled steel tubular columns were discussed. Kim *et al.* (2013), Hassanein and

Kharoob (2014) performed a parametric study and experimental studies on concrete-filled double skin columns, respectively. Based on the unified theory, Yu *et al.* (2013) proposed a unified formula that can be used in the design of the columns with various sections, including solid, hollow, circular and polygonal sections. Cascardi *et al.* (2016) presented a detailed summary of the existing analytical models and provided a unified procedure for concrete hollow columns restrained by FRP including both circular and square cross-sections. However, available studies of the composite action with difference hollow ratios on hollow concrete-filled circular steel tubular stub columns were limited.

In order to understand the confinement effect from steel tube on concrete in hollow concrete-filled circular steel tubular stub columns with difference hollow ratios, a total of 16 tests on hollow concrete-filled steel tubular stub columns under axial compression were conducted in this study. The effects of hollow ratio, concrete strength and thickness of steel tube on the mechanical behavior of the H-CFT columns were discussed based on the test results. With the aid of the nonlinear finite element software ABAQUS, a 3D finite element (FE) model was established with

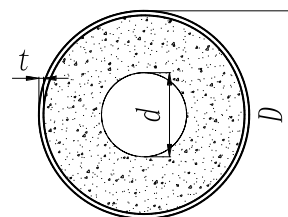


Fig. 1 Cross-section of H-CFT

*Corresponding author, Ph.D.,
E-mail: zhangtao0226@csu.edu.cn

Table 1 Properties of specimens and comparison between calculated results and tested ones

Specimen	$D \times d \times t$ / mm	L / mm	f_{cu} / MPa	f_s / MPa	ψ	ρ	$N_{u,e}$ / kN	$N_{u,1}$ / kN	DI
H-CFT1-A	302×49×3.76	900	37.7	308	0.028	0.052	3680	3528	6.586
H-CFT1-B	296×52×3.65				0.032	0.051	3520	3380	7.275
H-CFT2-A	300×52×3.72		52.4	308	0.032	0.052	4230	4317	6.706
H-CFT2-B	302×51×3.81				0.030	0.052	4560	4410	5.937
H-CFT3-A	294×113×3.62		37.7	308	0.155	0.051	3050	2991	5.911
H-CFT3-B	298×112×3.71				0.149	0.052	3150	3110	5.536
H-CFT4-A	301×110×3.78		52.4	308	0.141	0.052	4030	3937	4.997
H-CFT4-B	298×111×3.73				0.146	0.052	3950	3833	5.23
H-CFT5-A	301×202×3.64		37.7	308	0.473	0.05	2080	2121	4.087
H-CFT5-B	303×202×3.75				0.467	0.051	2200	2155	4.062
H-CFT6-A	297×201×3.69		52.4	308	0.482	0.052	2500	2610	2.703
H-CFT6-B	300×204×3.72				0.486	0.052	2520	2646	2.991
H-CFT7-A	299×199×5.82		37.7	311	0.480	0.083	2820	2779	4.977
H-CFT7-B	302×201×5.84				0.479	0.082	2800	2816	4.671
H-CFT8-A	298×203×5.78		52.4	311	0.486	0.082	3020	3150	3.548
H-CFT8-B	301×202×5.86				0.488	0.083	3100	3273	3.242

consideration of reasonable constitutive relation of concrete and steel material. The numerical model was validated by the test results and a parametric study regarding the influence of hollow ratio of H-CFT was further performed. Based on the results of tests and numerical analysis in this study together with those test data collected in literatures, a practical design formula for calculating the ultimate bearing capacity of H-CFT columns under axial compression was derived according to the limit equilibrium theory.

2. Experimental investigation

2.1 Materials and specimens

A total of 8 groups of H-CFT stub columns were designed for the tests in this study and the details are shown in Table 1. Each test has two identical specimens (namely A and B). D is the outer diameter of steel tube, d is the diameter of hollow part of the cross-section, t is the wall thickness of the steel tube and L is the height of the column specimen. f_{cu} is the cubic compressive strength of concrete, f_s is the yield strength of steel, ψ is the hollow area (A_{ci}) divided by the cross-section area without steel tube ($A_{ci} + A_c$) and ρ is the steel ratio of steel tube. $N_{u,e}$ is ultimate bearing capacity of H-CFT stub columns from experimental results, $N_{u,1}$ is ultimate bearing capacity of H-CFT stub columns from FE results and DI is the ductility index. Q235 steel plates with thicknesses of 4 mm and 6 mm respectively were used to carry out tensile coupon tests. The results on material properties of the two types of steel plates are shown in Table 2. f_u is ultimate strength of steel tube, E_s is elastic modulus of steel tube and v_{sc} ($\varepsilon_{\theta,s}/\varepsilon_{L,s}$) is strain ratio of steel tube. The steel tubes were manufactured by bending hot rolling steel plates into grooves and then welding the two edges along the longitudinal direction.

To prevent the steel tubes from rusting and obtain

Table 2 Properties of steel

Thickness	f_s / MPa	f_u / MPa	E_s / MPa	v_{sc}
4 mm	308	452	2.08×10^5	0.284
6 mm	311	460	2.08×10^5	0.285

a better observation of deformation of the specimens during test, red paint was sprayed on the outer surface of the steel tubes and grids of 50 mm × 50 mm were drawn on the painted surface. Before filling the concrete, the steel tube was welded with the bottom loading plate. The hollow part of the stub column specimen is made by the method of putting a PVC pipe with a specific diameter right inside at the center of the steel tube. A layer of lubricants was also applied to the outside of the PVC pipe. Concrete was poured from the top of the specimens and vibrated simultaneously with a vibrator to evenly distribute the concrete inside the steel tube. Finally, the top surface of concrete was smoothed for being at the same level with steel tube. The PVC pipe is gently removed half an hour after the concrete initial setting. Meanwhile, the standard concrete cubes with dimension of 150 mm were prepared and cured at the same condition as the test specimens. A concrete cube has been made after each specimen was poured. A total of 16 concrete cubes were tested at 28 day. The concrete surface of the column specimens was polished with grinder, and then brushed with a layer of epoxy resin binder. At finally, steel cover plates were placed at the top end of the H-CFT column specimens to guarantee that the steel tube and core concrete share loads from the initial loading stage.

2.2 Experimental setup and instrumentation

Axial compressive experiments on the H-CFT stub

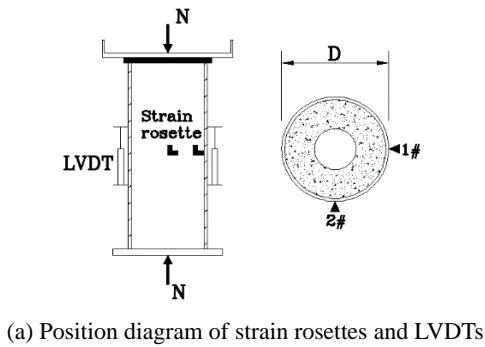


Fig. 2 Experimental instrumentation for all specimens

columns were conducted using a 500-ton tri-axial stress testing machine in the National Engineering Laboratory for High Speed Railway Construction at the Central South University. To accurately measure the deformation, two

strain rosettes (1# to 2# in Fig. 2) were attached at the mid-height of two adjacent side surfaces and two LVDTs with the range of 100 mm and accuracy of 0.1 mm (as shown in Fig. 2) were installed at the same height of two opposite side surfaces. Load-strain curves were acquired by a DH3818 static strain measurement system and load-deformation curves were recorded by the electronic transducers and data acquisition system.

The compressive load was applied from the top of the specimens using a load control mode. The test was carried out using load control in the elastic stage with a force increment of 1/20 of the expected ultimate load. After the load reached 60% of the expected ultimate bearing capacity, the test was switched to displacement control with an increment of 0.2 mm each step. Each loading step was sustained for 3-5 mins. When the ultimate load was approached, the specimens were loaded slowly and continuously until failure.

3. Experimental results and discussion

3.1 Load-deformation responses and failure modes

Fig. 3 shows the load-strain curves of the test specimens, which reveal that the compressive process of H-CFT stub columns can be divided into three phases: elastic stage, elastic-plastic stage and failure stage. Three different hollow diameters were designed for the test including $d = 50$ mm (H-CFT1 and H-CFT2), $d = 110$ mm (H-CFT3 and H-CFT4), and $d = 200$ mm (H-CFT5~H-CFT8). For the convenience of description, these three groups of specimens

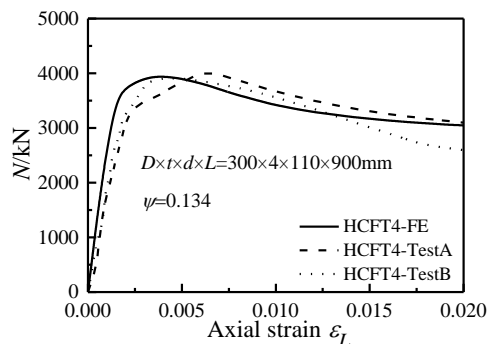
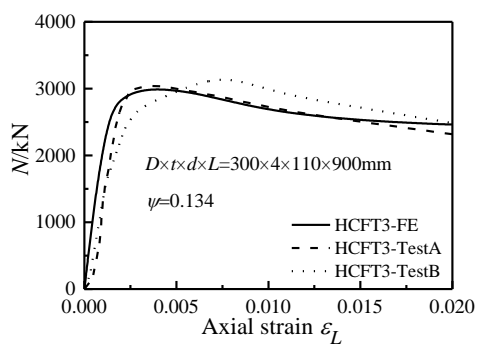
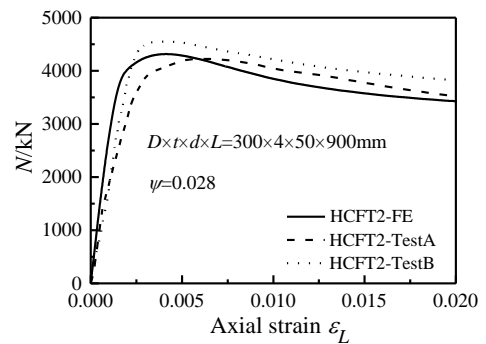
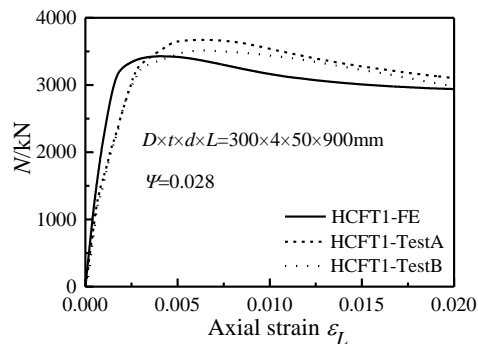


Fig. 3 Continued

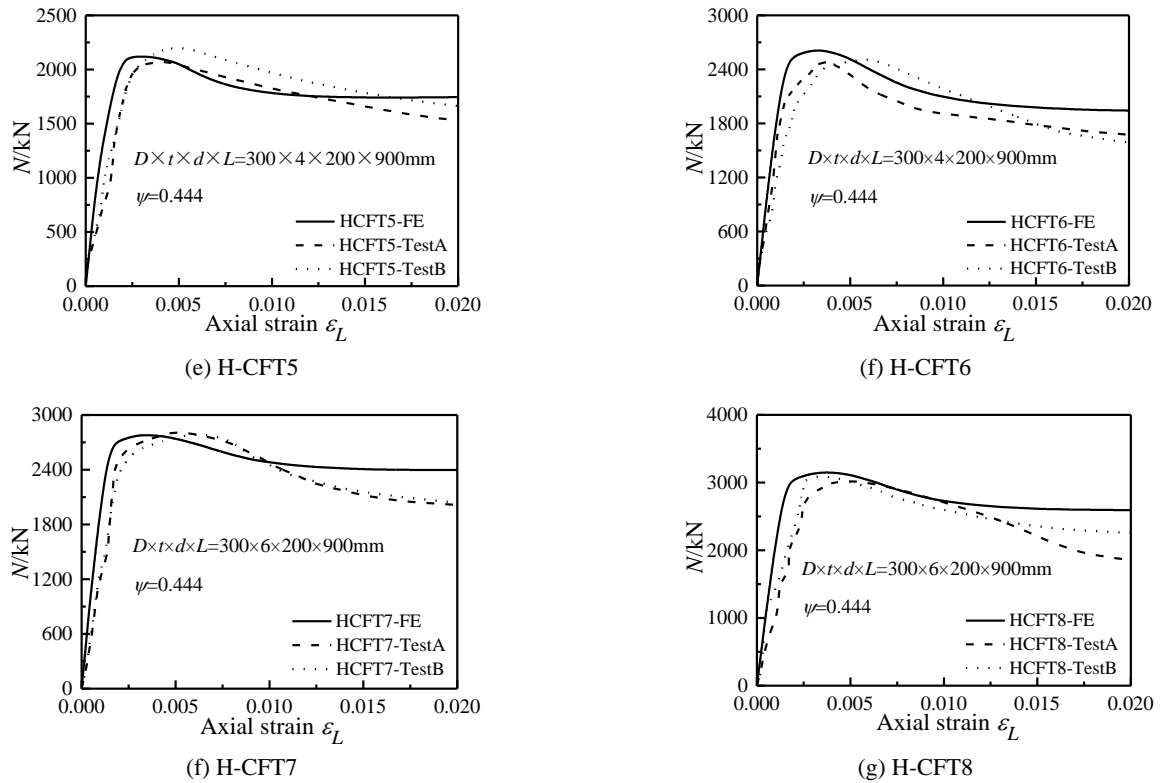


Fig. 3 Comparison of load-strain curves between FE and experimental results

were referred to as group A, group B, and group C, respectively. The experimental phenomena of the stub columns in different groups are different all through the compression process.

At the initial loading stage, all the specimens are in the elastic stage, which is reflected by the linear responses of the load-strain curves, as shown in Fig. 3. The compressive stiffness of the specimens in this stage is larger than that in the other stages, and the axial displacement is very small.

The specimens appear obvious plastic deformation after entering the elastic-plastic stage. For the specimens in group A with small hollow ratios, the confinement effect of steel tube on concrete is not obviously weakened. While for the specimens in group B with medium hollow ratios, there is no restraint on the inside of the concrete and the sound of concrete falling off can be heard at the elastic-plastic stage. Moreover, the load-strain curves for the specimens in group C with the largest hollow ratios ascend most slowly at the

elastic-plastic stage and the sound of concrete falling off can be heard continuously. It is demonstrated that the confinement effect from the steel tube on the concrete for the specimens in group A is strongest compared to group B and group C.

When the ultimate load was approached, the buckling deformation of specimens in group A occurred near the mid-height of the stub columns and the load-strain curves began to descend gently before reaching a stable value. However, the buckling deformation of specimens in group B appeared near the end of the stub columns and load-strain curves decreased obviously after the ultimate load was reached. Furthermore, the buckling deformation of specimens in group C appeared just at the end of the stub columns and load-strain curves decreased rapidly after the ultimate load was reached.

Comparing the FE results and experimental data in Fig. 3, it is noted that the FE model predicts higher initial



(a) Comparison of steel tube buckling



(b) Comparison of concrete failure

Fig. 4 Typical failure modes of specimens

stiffness when compare with the experimental results. This phenomenon may be mainly caused by the following reasons. (1) The contact between the loading plate and the end of the specimen is not dense enough, which leads to the shift of the test curve at the beginning, however, the stiffness of FE results and experimental data achieve the same level later (such as Figs. 3(c), (e)). (2) The cube strength is measured first and column is tested later, this leads to the difference between the tested cube strength and concrete strength inside the column. (3) Because of the existence of the hollow part, the compactness of concrete is worse than that of solid concrete and the inward collapse of concrete under compression.

Fig. 4 shows the typical failure modes of the tested specimens. The supporting function of the concrete on the steel tubes reduced with the increase of hollow ratio and the buckling position of the steel tubes moved from the middle portion (group A) gradually to the end (group C) of the stub columns when the specimens failed, as shown in Fig. 4(a). On the other hand, with the increase of hollow ratio, the confinement effect from steel tube on concrete is also weakened and the shedding degree of concrete is increased with the increase of hollow ratio, as shown in Fig. 4(b).

3.2 Bearing capacity

Fig. 5 shows the experimental results of the ultimate bearing capacities of all specimens. In comparison with H-CFT5 ($f_s = 308$ MPa, $f_{cu} = 37.70$ MPa, $\rho = 0.051$), the average ultimate bearing capacity of H-CFT7 ($f_s = 311$ MPa, $f_{cu} = 37.70$ MPa, $\rho = 0.082$) specimens improved by 31.31%. The comparison between H-CFT6 ($f_s = 308$ MPa, $f_{cu} = 52.4$ MPa, $\rho = 0.052$) and H-CFT8 ($f_s = 311$ MPa, $f_{cu} = 52.4$ MPa, $\rho = 0.083$) reveals that the average ultimate bearing capacity only improved by 21.91% with the same increase of steel ratio as the former comparison. It is therefore concluded that increasing the steel ratio can contribute to the improvement of load bearing capacity, and the effect is more significant for the H-CFT columns with lower concrete strength.

The comparison of the average ultimate bearing capacities of H-CFT5 ($f_s = 308$ MPa, $f_{cu} = 37.70$ MPa, $\rho =$

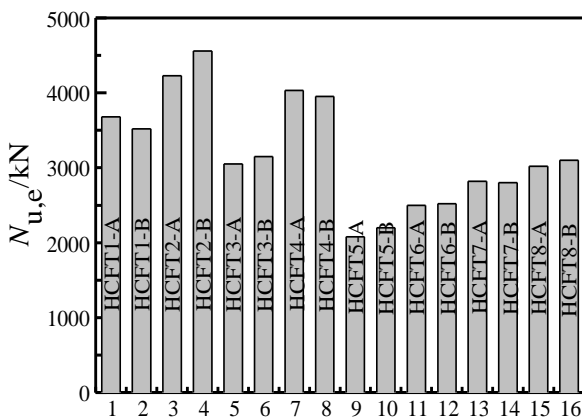


Fig. 5 Comparison of ultimate bearing capacities for all specimens

0.051) with H-CFT6 ($f_s = 308$ MPa, $f_{cu} = 52.4$ MPa, $\rho = 0.052$) shows that the ultimate bearing capacity of H-CFT6 improved by 42.5% with the increase of concrete strength. However, the comparison between H-CFT7 ($f_s = 311$ MPa, $f_{cu} = 37.70$ MPa, $\rho = 0.082$) and H-CFT8 ($f_s = 311$ MPa, $f_{cu} = 52.4$ MPa, $\rho = 0.083$) reveals that the average ultimate bearing capacity of H-CFT8 specimens only improved by 8.90% with the same increase of concrete strength as the former comparison. It is indicated that the increase of concrete strength can improve of load bearing capacity, and the effect is more significant for the H-CFT columns with smaller steel ratio based on the results in this study.

The comparison of the average ultimate bearing capacities of H-CFT5 ($\psi = 0.470$) with H-CFT3 ($\psi = 0.152$) shows that the ultimate bearing capacity of H-CFT5 reduced by 30.97% with the increase of hollow ratio. The comparison between H-CFT3 ($\psi = 0.152$) and H-CFT1 ($\psi = 0.030$) reveals that the average ultimate bearing capacity of H-CFT3 specimens reduced by 13.89%. Moreover, the comparison of H-CFT6 ($\psi = 0.484$) and H-CFT4 ($\psi = 0.143$) shows that the ultimate bearing capacity of H-CFT6 reduced by 37.09% with the increase of hollow ratio. The comparison between H-CFT4 ($\psi = 0.143$) and H-CFT2 ($\psi = 0.031$) reveals that the average ultimate bearing capacity of H-CFT3 specimens reduced by 9.22%. It is therefore concluded that the increase of hollow ratio can lead to a decrease of load bearing capacity, and the effect is more significant when the hollow ratio is large.

3.3 Ductility

In order to investigate the effect of concrete strength and steel ratio on the ductility of H-CFT specimens, a ductility index (DI), which has been used for studying the internal constrained square CFTs in Ding *et al.* (2014), is adopted in this paper and the corresponding ductility index is defined as follows

$$DI = \frac{\varepsilon_{0.85}}{\varepsilon_b} \quad (1)$$

where $\varepsilon_{0.85}$ is the axial strain when the load falls to 85% of the ultimate load; ε_b is equal to $\varepsilon_{0.75}/0.75$, and $\varepsilon_{0.75}$ is the axial strain when the load attains of 75% the ultimate load

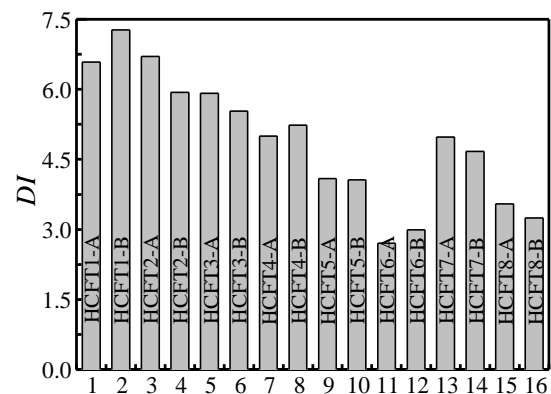


Fig. 6 Comparison of ductility index (DI) for all specimens

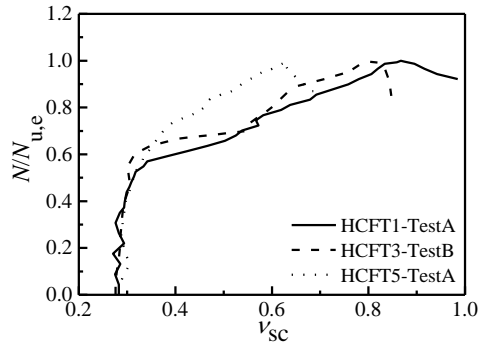


Fig. 7 Comparison of load-transverse strain curves

in the pre-ultimate stage. The ductility coefficients calculated by Eq. (1) for all specimens are shown in Table 1.

Fig. 6 shows the experimental results of DI for all the specimens, among which a larger value of DI indicates a slower process of load reduction in the post-ultimate stage. Based on the comparison results between H-CFT1 and H-CFT2, H-CFT3 and H-CFT4, H-CFT5 and H-CFT6, as well as H-CFT7 and H-CFT8, the DI value is reduced with the increase of concrete strength. Moreover, the comparisons of specimens H-CFT7 vs. H-CFT5, and H-CFT8 vs. H-CFT6, the DI value increases by 18.4% and 19.2% on average with the increasing steel ratio. Finally, the comparison of the DI values of H-CFT5, H-CFT3 and H-CFT1 shows that the DI is reduced with the increase of hollow ratio.

3.4 Strain ratio

Fig. 7 shows the relationship of the normalized axial load ($N/N_{u,c}$) against the strain ratio (v_{sc}) of H-CFT1, H-CFT3 and H-CFT5 specimens. The strain ratio, which is defined as the absolute value of the circumferential strain divided by the axial strain of the steel tube at each gauged points, represents the composite action between the steel tube and the core concrete. The larger the strain ratio is, the more composite action is between them.

It can be observed from Fig. 7 that at the initial loading stage, the strain ratio remains constant and almost equals to the Poisson's ratio of steel. It is indicated that there is nearly no composite action between the steel tube and core concrete. After the applied load reaches around 60% of the ultimate bearing capacities of the specimens, the strain ratio increases significantly, which indicate an obvious confinement effect of the steel tube on the core concrete. The strain ratio of specimen H-CFT1-A is the largest while that of specimen H-CFT5-A is the smallest among the three specimens at the same load level. It is demonstrated that the composite action between the steel tube and the core concrete decreases with the increase of hollow ratio.

4. Finite element (FE) modeling

4.1 FE models

FE models of the H-CFT stub columns were established

using ABAQUS/Standard 6.10. In these models, 4-node shell elements (S4R) with reduced integration were adopted for the steel tubes of all specimens. Moreover, 9-node Simpson integration was adopted along the thickness of the shell elements to improve the accuracy of calculation. The 8-node reduced integral format 3D solid elements (C3D8R) were used to model the core concrete and loading plate, and the surface of the loading plate was defined as rigid to ensure that the deformation of the upper and lower surfaces of steel tube and concrete was the same. A structured meshing option with a mesh size of 50 mm was adopted, and the resulting FE model is shown in Fig. 8.

A tie constraint may couple two separate surfaces together so that no relative motion occurs between them. Therefore, the tie option was adopted for the constraint between the concrete and the loading plate. Shell-to-solid coupling is a surface-based technique for coupling shell elements (steel tube) to solid elements (loading plate) and it was adopted for the constraint between the steel tube and the loading plate. A pure master-slave surface contact was adopted for the constraint between the steel tube (master surface) and the core concrete (slave surface).

The following non-dimensional mathematical form for the stress-strain relationship of concrete under uniaxial compression, as proposed in Ding *et al.* (2011a), was used for the material model of concrete in this study

$$y = \begin{cases} \frac{kx + (m-1)x^2}{1 + (k-2)x + mx^2} & x \leq 1 \\ \frac{x}{\alpha_1(x-1)^2 + x} & x > 1 \end{cases} \quad (2)$$

where $y (= \sigma/f_c)$ and $x (= \varepsilon/\varepsilon_c)$ are the stress and strain ratio of the core concrete, respectively; σ and ε are the stress and strain of the core concrete; $f_c (= 0.4f_{cu}^{7/6})$ is the uniaxial compressive strength of concrete, where f_{cu} is the compressive strength of standard cubic concrete with dimension of 150 mm; ε_c is the strain corresponding with the peak compressive stress of concrete, where $\varepsilon_c = 383f_{cu}^{7/18} \times 10^{-6}$. The parameter k is the ratio of the initial tangent modulus to the secant modulus at peak stress; $m = 1.6(k-1)^2$ is a parameter that controls the decrease in the elastic modulus along the ascending branch of the axial stress-strain relationship. For a concrete-filled steel tubular stub column, the parameter α_1 is taken as 0.15.

The following expression for the stress-strain relationship of steel, as detailed in Ding *et al.* (2011a), was adopted for the material model of steel in this study



(a) Whole FE model (b) Concrete element (c) Steel element

Fig. 8 Mesh generation of the numerical model

$$\sigma_i = \begin{cases} E_s \varepsilon_i & \varepsilon_i \leq \varepsilon_y \\ f_s & \varepsilon_y < \varepsilon_i \leq \varepsilon_{st} \\ f_s + \zeta E_s (\varepsilon_i - \varepsilon_{st}) & \varepsilon_{st} < \varepsilon_i \leq \varepsilon_u \\ f_u & \varepsilon_i > \varepsilon_u \end{cases} \quad (3)$$

where, σ_i and ε_i are the equivalent stress and strain of the steel tube, respectively; f_s, f_u ($= 1.5f_s$) and E_s ($= 2.06 \times 10^5$ MPa) are the yield strength, ultimate strength, and elastic modulus of steel, respectively; $\varepsilon_s, \varepsilon_{st}$ and ε_u are the yield strain, hardening strain, and ultimate strain of steel, in which $\varepsilon_{st} = 12\varepsilon_s$ and $\varepsilon_u = \varepsilon_{st} + 0.5f_s/(\zeta E_s) = 120\varepsilon_s$. The parameter ζ is taken as 1/216.

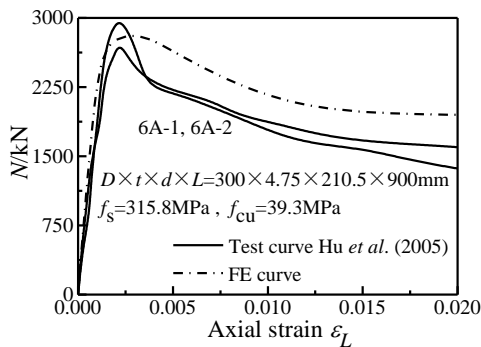


Fig. 9 Comparisons between the calculated and test curves of load-strain relations

In order to model the decrease of load-bearing capacity of the specimens, the load is applied to the column models using the displacement method. Both the material and structural nonlinearities were considered and the FE analysis was solved using the incremental-interactive method in ABAQUS.

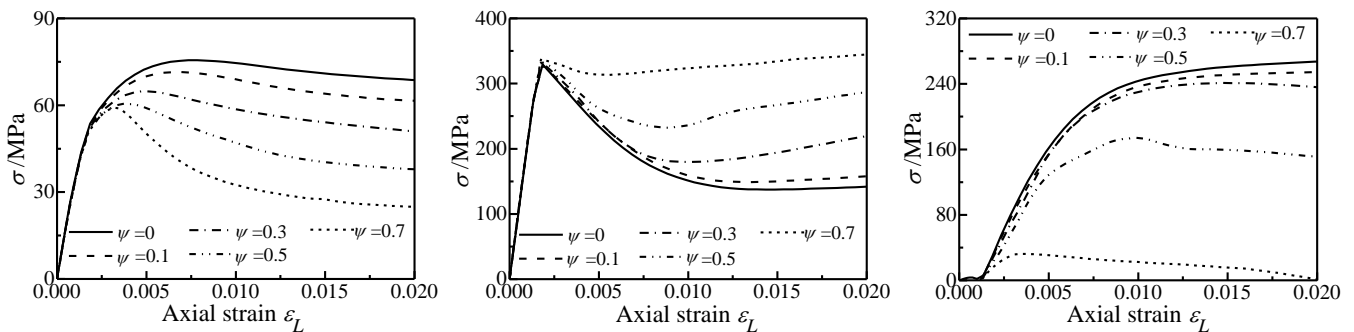
4.2 Results and discussion

The load-axial strain curves of H-CFT stub columns obtained from FE analysis and available experimental results in literatures (Hu et al. 2005) are shown in Fig. 9. The experimental results ($N_{u,e}$) of 38 H-CFT stub columns under axial compression in literatures (Hu et al. 2005, Kuranova and Kvedaras 2007, Yu et al. 2013) and the finite element results ($N_{u,1}$) were also compared and summarized in Table 3. It is shown that good agreement was achieved between the experimental and FE modeling results. So the FE analysis method is proved to be correct.

In order to analyze the effect of hollow ratio on the mechanical behavior (through various stresses) of different parts of the H-CFT stub columns, a parametric study was performed using the validated FE model. The parameters of the H-CFT stub columns in the parametric study include $D = 300$ mm, $t = 6$ mm, $L = 900$ mm, $\psi = 0, 0.1, 0.3$, or $0.5, 0.7$, $f_{cu} = 60$ MPa, $f_s = 345$ MPa. Fig. 10 shows the comparison of the stress-strain relationship for the H-CFT stub columns with different hollow ratios obtained from the parametric study. The stresses include the average longitudinal stress of the core concrete, the longitudinal and

Table 3 Comparison between the FE results and tested oners of H-CFT specimens

Reference	D (mm)	t (mm)	d (mm)	L/D	f _s (MPa)	f _{cu} (MPa)	N _{u,e} /N _{u,1}		Sum
							Avg.	Dispersion coefficient	
Kuranova and Kvedaras (2007)	219-220	4.9-5.0	153-156	1.99-2.00	361.0	33.39	0.997	0.009	3
Hu et al. (2005)	300	2.5-4.8	211-235	3.00	315.8-334.6	37.57-59.85	1.170	0.085	9
Yu et al. (2013)	200-296	2.0-4.7	138-202	3.00-3.04	171.5-300.0	50.77-82.47	1.044	0.060	26
This study	300	4.0-6.0	50-200	3.00	308-311	37.70-52.40	1.001	0.033	16
Sum	166-360	2.0-6.0	41-256	2.50-3.08	171.5-361.0	33.39-82.47	1.040	0.053	54



(a) Average longitudinal stress-strain relationship of the core concrete (b) Longitudinal stress-strain relationship of the steel tube (c) Circumferential stress-strain relationship of the steel tube

Fig. 10 Comparison of the stress-strain relationship with different hollow ratios

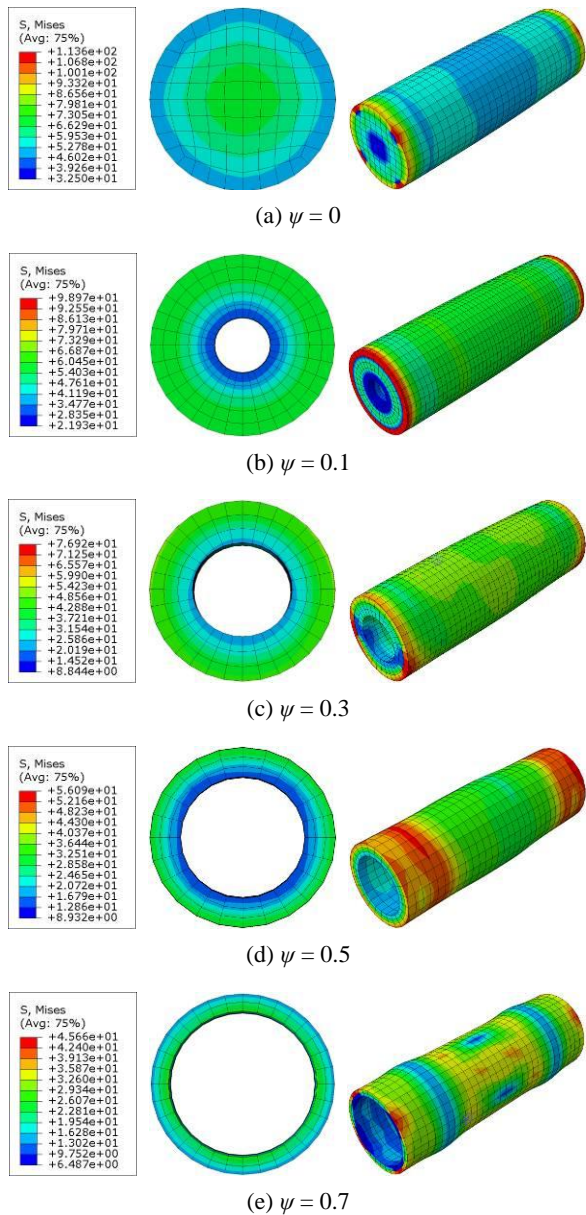


Fig. 11 Stress and deformation contour of concrete elements for H-CFT models with different hollow ratios

the circumferential stress of the steel tube. Fig. 11 shows the stress and deformation contour of concrete elements for H-CFT models with different hollow ratios. It is shown that when the stub columns are solid, the cross-sectional stress of the concrete elements increases gradually from the outside to the inside. However, when the stub columns are hollow, the cross-sectional stress decreases gradually from the inside to the outside. The results of the parametric study show:

- (a) Compared with the solid concrete-filled steel tubular stub columns (CFST), the peak value of the average longitudinal stress of the core concrete in H-CFT was reached earlier and gradually decreased with the increase of the hollow ratio. Moreover, the decreasing rate of longitudinal stress is accelerated, as shown in Fig. 10(a);

- (b) After the yield of steel tube, the reduction rate of the longitudinal stress in the steel tube slowed down with the increase of hollow ratio as shown in Fig. 10(b). Besides, the hoop stress is reduced with the increase of hollow ratio. Moreover, the circumferential stress of the steel tube is reduced after the peak value when the $\psi \geq 0.5$, as shown in Fig. 10(c);
- (c) The failure modes of the specimens with various hollow ratios are different, e.g., the H-CFT stub column with $\psi = 0.7$ was failed by obvious buckling of the steel tube, as shown in Fig. 11(e). It is indicated that the confinement effect from the steel tube on the core concrete is weakened with the increase of hollow ratio.
- (d) The increase of the circumferential stress of the steel tube is due to the extrusion of the core concrete to the steel tube. The increase of the circumferential stress of the steel tube indicates that the confinement of the steel tube on the core concrete is strengthened. With the increase of the hollow ratio ψ , the decrease of the circumferential stress of the steel tube in Fig. 10(c) indicates that the confining stress of the steel tube is reduced and the confinement effect is weakened.

5. Bearing capacity calculation

5.1 Formulation

Based on the theory of static equilibrium, the axial ultimate bearing capacity N_u can be determined using the equation below. It should be mentioned that the radial stress of the steel tube is ignored at the ultimate state.

$$N_u = \sigma_{L,c} A_c + \sigma_{L,s} A_s \quad (4)$$

where, $\sigma_{L,c}$ is the longitudinal stress of core concrete, $\sigma_{L,s}$ is longitudinal stress of steel tube, A_s is the cross-sectional area of steel tube, A_c is the cross-sectional area of core concrete;

The axial compressive strength of core concrete in constrained area is

$$\sigma_{L,c} = f_c + p \sigma_{r,c} \quad (5)$$

where, p is the lateral pressure coefficient, f_c is axial compressive strength of core concrete, $\sigma_{r,c}$ is radial stress of concrete.

According to the expressions of stresses for concrete and steel obtained from elasto plastic analysis in Ding *et al.* (2011b), the relationship between $\sigma_{r,c}$ and $\sigma_{\theta,s}$ can be derived as

$$\sigma_{r,c} = \frac{\rho(d_c^2 - d^2)}{(1 - \rho)2d_c^2} \sigma_{\theta,s} \quad (6)$$

where ρ is the steel ratio of cross-section, $\rho = A_s/A_{sc}$, $\sigma_{\theta,s}$ is the transverse stress of the steel tube; d_c is the diameter of concrete section encircled by an arbitrary point, $d \leq d_c \leq D_c$. When $d_c = D_c$ (D_c is outer diameter of concrete)

Table 4 Formulae sourced from the literatures for ultimate bearing capacity of H-CFT stub columns

Order	Reference	Formula
1	Yu <i>et al.</i> (2013)	$N_u = A_{sc}(1 + 1.5k\zeta)f_{ck} / (1 + B\zeta)$; $A_{sc} = A_s + A_c$, $k = 2k_e / 3 + 1/3$, $k_e = 1.0$, $B = f_{ck} / f_y$ (16)
2	Kvedaras and Sapalas (1999)	$N_{pl,Rd} = N_{su} + N_{cu}$; $N_{su} = 1.074f_yA_s$, $N_{cu} = 1.32f_{ck}A_c$ (17)
3	Hu <i>et al.</i> (2005)	$N_u = A_{sc}[(1.212 + B\zeta_o + C\zeta_o^2) - k\psi\zeta] 1.1f_{ck}$; $A_{sc} = A_s + A_c$, $\zeta_o = A_s f_y / (1.1A_c f_{ck})$, $k = 0.2$, $\psi = A_{ci} / A_{co}$, $\zeta = A_s f_y / (1.1A_c f_{ck})$, $B = 0.1759f_y / 235 + 0.974$, $C = -0.1038f_{ck} / 20 + 0.0309$ (18)

Table 5 Comparisons between calculated values and test results of H-CFT specimens

Sample size (Ref.)	Statistical eigenvalue	$N_{u,e} / N_{u,1}(N_{u,2})$				
		FE	Eq. (14)	Eq. (16)	Eq. (17)	Eq. (18)
16 (This study)	Average.	1.001	0.968	0.912	0.841	0.867
	Dispersion coefficient	0.033	0.030	0.161	0.172	0.207
26 (Yu <i>et al.</i> 2013)	Average.	1.044	0.996	1.069	1.005	1.079
	Dispersion coefficient	0.060	0.056	0.070	0.048	0.097
3 (Kuranovas and Kvedaras 2007)	Average.	0.997	0.987	0.761	0.928	1.395
	Dispersion coefficient	0.009	0.007	0.003	0.005	0.033
9 (Hu <i>et al.</i> 2005)	Average.	1.170	1.090	0.979	1.010	1.235
	Dispersion coefficient	0.085	0.081	0.070	0.071	0.128
Ψ Sample size						
≤ 0.1	Average.	1.013	0.992	1.022	0.976	0.922
10	Dispersion coefficient	0.027	0.026	0.108	0.146	0.137
≤ 0.3	Average.	1.020	0.978	1.032	0.958	0.963
10	Dispersion coefficient	0.047	0.041	0.100	0.094	0.098
≤ 0.5	Average.	1.006	0.979	0.975	0.924	1.003
14	Dispersion coefficient	0.045	0.043	0.101	0.104	0.127
≤ 0.7	Average.	1.088	1.034	0.943	0.984	1.211
20	Dispersion coefficient	0.082	0.085	0.107	0.079	0.129
Sum	Average.	1.040	1.000	0.984	0.960	1.053
54	Dispersion coefficient	0.053	0.064	0.104	0.099	0.122

*Note: $N_{u,e}$ is experimental results; $N_{u,1}$ is the FE results; $N_{u,2}$ is the formula calculation values

$$\sigma_{\theta,s} = \frac{2(1-\rho)}{\rho(1-\psi)} \sigma_{r,c} \quad (7)$$

$$N_u = A_c f_c \left[1 + \left(p - \frac{1}{1-\psi} \right) \frac{\sigma_{r,c}}{f_c} + \sqrt{\Phi^2 - \frac{3}{(1-\psi)^2} \left(\frac{\sigma_{r,c}}{f_c} \right)^2} \right] \quad (10)$$

$\psi = A_{ci}/A_{co}$; A_{co} is area surrounded by steel tube, $A_{co} = A_{ci} + A_c$; A_{ci} is area of the hollow part.

For steel pipes, the following equation can be obtained by Von Mises yield criterion

$$\sigma_{L,s}^2 + \sigma_{L,s} \sigma_{\theta,s} + \sigma_{\theta,s}^2 = f_s^2 \quad (8)$$

When the steel tube is at the ultimate limit state, the longitudinal stress of steel tube $\sigma_{L,s}$ can be expressed as

$$\sigma_{L,s} = \sqrt{f_s^2 - \frac{3}{4} \sigma_{\theta,s}^2} - \frac{1}{2} \sigma_{\theta,s} \quad (9)$$

Substituting Eqs. (5), (7) and (9) into Eq. (4), N_u can be obtained by

in which Φ is determined as

$$\Phi = \frac{f_s A_s}{f_c A_c} \quad (11)$$

At the limit equilibrium state, there is

$$\frac{dN_u}{d\sigma_{r,c}} = 0 \Rightarrow \frac{\sigma_{r,c}}{f_c} = \frac{\Phi(p-e)}{e\sqrt{9e^2 + 3(p-e)^2}} \quad (12)$$

where e is determined as: $e = 1/(1-\psi)$.

Substituting Eq. (12) into Eq. (10), the ultimate bearing capacity of H-CFT can be determined by

$$N_{u,max} = A_c f_c \left[1 + \Phi \sqrt{\frac{3 + (p(1-\psi)-1)^2}{3}} \right] \quad (13)$$

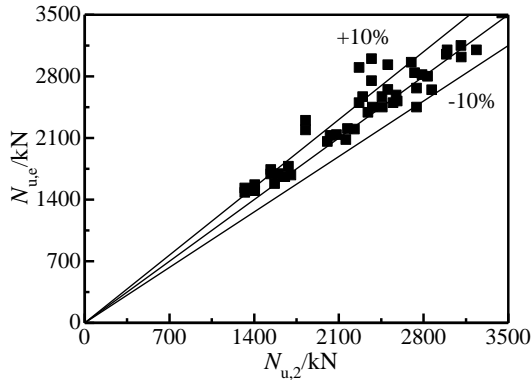


Fig. 12 Comparisons between the calculated value of Eq. (14) and test results

According to the reference Ding *et al.* (2011b), $p = 3.4$. Therefore, Eq. (13) of the ultimate bearing capacity can be simplified as the equation below when the value of ψ ranges from 0 to 0.7

$$N_{u,\max} = A_c f_c [1 + (1.7 - 1.7\psi + \psi^2)\Phi] \quad (14)$$

When $\psi = 0$, the calculation formula (14) of the ultimate bearing capacity can be further simplified as

$$N_{u,\max} = A_c f_c (1 + 1.7\Phi) \quad (15)$$

It can be seen that Eq. (15) is identical to the calculation formula for the ultimate bearing capacity of concrete-filled steel tubular stub columns under axial compression. Therefore, it can be regarded that Eq. (14) is an extension of the calculation formula for the bearing capacity of concrete-filled steel tubular columns under axial compression.

5.2 Comparisons

Table 4 lists the different design formulae for the ultimate bearing capacity of H-CFT stub columns under axial compression. The comparison of experimental results, the FE results, and the predicted values using Eq. (14) and the formulae in Table 4 is shown in Table 5.

The comparison in Table 5 shows that:

- The ultimate bearing capacities obtained from the finite element analysis and Eq. (14) is in good agreement with the experimental values;
- When the hollow ratio of the H-CFT stub columns is less than 0.5, the predicted strengths by Eq. (14) are more close to the experiment results with a smaller dispersion coefficient compared with other formulas;
- The predicted strengths by Eq. (14) proposed in this study and Eq. (16) existing in the standard are close, but the dispersion of the former is smaller compared to the experimental results.

Fig. 12 shows the comparison between the calculated results ($N_{u,2}$) by Eq. (14) and the test values ($N_{u,e}$). The comparison between the calculated results ($N_{u,2}$) by Eq. (14) and the finite element results ($N_{u,1}$) is also plotted in Fig. 13.

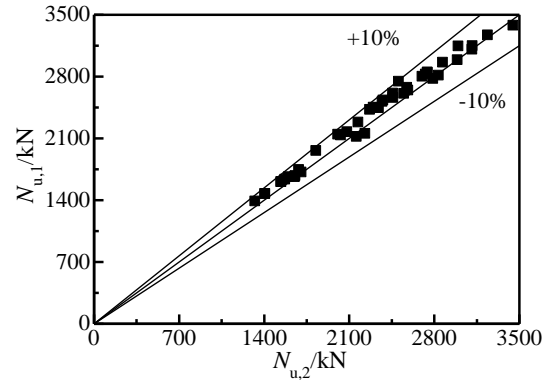


Fig. 13 Comparison between the calculated values of Eq. (14) and finite element results

It is shown that the calculated results using the design formulae for H-CFT stub columns proposed in this study are generally in good agreement with the experimental and finite element results.

6. Conclusions

- A total of 16 tests on hollow concrete-filled circular steel tubular stub columns under axial compression were conducted in this study. The effects of hollow ratio, concrete strength and thickness of steel tube on the mechanical behavior of the H-CFT columns were discussed based on the test results. It is found that the increase of hollow ratio can lead to a decrease of load bearing capacity, and the effect is more significant when the hollow ratio is large.
- A3D finite element (FE) model was established with consideration of reasonable constitutive relation of concrete and steel material. The numerical model was validated by the test results and a parametric study regarding the influence of hollow ratio of H-CFT was further performed.
- The parametric study results show that the failure modes of the specimens with various hollow ratios are different, and the H-CFT section generally becomes more slender with the increase of hollow ratio. It is also indicated that the confinement effect from the steel tube on the core concrete is weakened with the increase of hollow ratio.
- Based on the results of tests and numerical analysis, a practical design formula for calculating the ultimate bearing capacity of H-CFT columns under axial compression was derived according to the limit equilibrium theory. It is demonstrated that the calculated results using the proposed formula are in good agreement with the experimental results.

Acknowledgments

This research work was financially supported by a grant from the National Key R&D Plan of China (Grant No. 2017YFC0703404). The financial support is highly appreciated.

References

- Aslani, F., Uy, B., Tao, Z. and Mashiri, F. (2015), "Predicting the axial load capacity of high-strength concrete filled steel tubular columns", *Steel Compos. Struct., Int. J.*, **19**(4), 967-993.
- Aslani, F., Uy, B., Wang, Z. and Patel, V. (2016), "Confinement models for high strength short square and rectangular concrete-filled steel tubular columns", *Steel Compos. Struct., Int. J.*, **22**(5), 937-974.
- Albaredavalls, A. and Carreras, J.M. (2015), "Efficiency of stiffening plates in fabricated concrete-filled tubes under monotonic compression", *Steel Compos. Struct., Int. J.*, **18**(4), 1023-1044.
- Chang, X., Fu, L., Zhao, H.B. and Zhang, Y.B. (2013), "Behaviors of axially loaded circular concrete-filled steel tube (CFT) stub columns with notch in steel tubes", *Thin-Wall. Struct.*, **73**(12), 273-280.
- Chang, X., Luo, X., Zhu, C. and Tang, C. (2014), "Analysis of circular concrete-filled steel tube (CFT) support in high ground stress conditions", *Tunn. Undergr. Space Technol.*, **43**(7), 41-48.
- Cascardi, A., Micelli, F. and Aiello, M.A. (2016), "Unified model for hollow columns externally confined by FRP", *Eng. Struct.*, **111**, 119-130.
- Ding, F.X., Ying, X.Y. and Zhou, L.C. (2011a), "Unified calculation method and its application in determining the uniaxial mechanical properties of concrete", *Front. Archit. Civ. Eng. China.*, **5**(3), 381-393.
- Ding, F.X., Yu, Z.W. and Bai, Y. (2011b), "Elasto-plastic analysis of circular concrete-filled steel tube stub columns", *J. Struct. Eng.*, **67**(10), 1567-1577.
- Ding, F.X., Fang, C.J., Bai, Y. and Gong, Y.Z. (2014), "Mechanical performance of stirrup-constrained concrete-filled steel tubular stub columns under axial loading", *J. Constr. Steel Res.*, **98**(11), 146-157.
- Ellobody, E. (2013a), "Numerical modelling of fibre reinforced concrete-filled stainless steel tubular columns", *Thin-Wall. Struct.*, **63**, 1-12.
- Ellobody, E. (2013b), "Nonlinear behaviour of eccentrically loaded FR concrete-filled stainless steel tubular columns", *J. Constr. Steel Res.*, **90**, 1-12.
- Feng, P., Cheng, S., Bai, Y. and Ye, L. (2015), "Mechanical behavior of concrete-filled square steel tube with frp-confined concrete core subjected to axial compression", *Compos. Struct.*, **123**(5), 312-324.
- Hassanein M.F. and Kharoob, O.F. (2014), "Analysis of circular concrete-filled double skin tubular slender columns with external stainless steel tube", *Thin-Wall. Struct.*, **79**(6), 23-37.
- Hua, W., Wang, H.J. and Hasegawa, A. (2014), "Experimental study on reinforced concrete filled circular steel tubular columns", *Steel Compos. Struct., Int. J.*, **17**(4), 517-533.
- Hu, Q.H., Xu, G.L. and Wang, H.W. (2005), "The strength calculation of various centrifugal hollow concrete filled steel tube (H-CFST) members under compression", *J. Harbin Inst. Tech.*, **37**(Sup.), 149-152. [In Chinese]
- Kvedaras, A.K. and Sapalas, A. (1999), "Research and practice of concrete-filled steel tubes in Lithuania", *J. Constr. Steel Res.*, **49**(2), 197-212.
- Kuranovas, A. and Kvedaras, A.K. (2007), "Behaviour of hollow concrete-filled steel tubular composite elements", *J. Civ. Eng. Manage.*, **13**(2), 131-141.
- Kim, J.K., Kwak, H.G. and Kwak, J.H. (2013), "Behavior of hybrid double skin concrete filled circular steel tube columns", *Steel Compos. Struct., Int. J.*, **14**(2), 191-204.
- Lai, M.H. and Ho, J.C.M. (2013), "Uni-axial compression test of concrete-filled-steel-tube columns confined by tie bars", *Proc. Eng.*, **57**(1), 662-669.
- Patel, V.I., Uy, B., Prajwal, K.A. and Aslani, F. (2016), "Confined concrete model of circular, elliptical and octagonal cfst short columns", *Steel Compos. Struct., Int. J.*, **22**(3), 497-520.
- Qu, X., Chen, Z. and Sun, G. (2015), "Axial behaviour of rectangular concrete-filled cold-formed steel tubular columns with different loading methods", *Steel Compos. Struct., Int. J.*, **18**(1), 71-90.
- Yu, M., Zha, X.X., Ye, J.Q. and Li, Y.T. (2013), "A unified formulation for circle and polygon concrete-filled steel tube columns under axial compression", *Eng. Struct.*, **49**(2), 1-10.

CC